doi: 10.37905/jgeosrev.v8i2.36629 ejurnal.ung.ac.id/index.php/jgeosrev

Vol. 8, No. 2, July 2026: 163-174

Jambura Geoscience Review

p-ISSN 2623-0682 | e-ISSN 2656-0380

Department of Earth Science and Technology, Universitas Negeri Gorontalo

Tidal Flood Mapping Based on Land Use Classification Using CDAT and Deep Learning in Sayung, Demak

Muchamad Syaoqi Ilham Setiawan[1], Arifin Septian Nugroho[1], Nurhadi Bashit[1], Hana Sugiastu Firdaus[1], Abdi Sukmono[1]

[1] *Geodetic Engineering Study Program, Diponegoro University, Jl. Prof. Soedarto, Semarang, 50275, Indonesia*

ARTICLE INFO

Article history:
Received: 03 January 2026
Accepted: 19 June 2026
Published: 03 July 2026

Keywords:
CDAT; Deep Learning; Land Use; Sayung District; Tidal Flooding

Corresponding author:
Nurhadi Bashit
Email:
nurhadi.bashit@live.undip.ac.id

ABSTRACT

Comprehensive spatial impact analysis integrating flood detection with land use classification has remained limited despite the occurrence of escalating tidal flooding that threatens coastal communities, aquaculture zones, and agricultural lands in the Sayung District. This study aimed to assess and map the spatial distribution of tidal flooding and analyze its impacts on land use through integrated remote sensing and artificial intelligence methodologies. The change detection and thresholding (CDAT) method utilizing Sentinel-1A imagery was employed for tidal flood detection, whereas the U-net deep learning architecture with stacked Sentinel-1A and Sentinel-2A data was implemented for multiclass land use classification. The CDAT method successfully detected 14.636 km² of inundated area, representing 12.25% of the Sayung District, with an overall accuracy of 0.886 and a kappa coefficient of 0.755. The U-net model classified 11 land use categories with an overall accuracy of 0.81 and a kappa coefficient of 0.78, demonstrating robust performance, particularly for aquaculture ponds and cultivated aquatic, with IoU values exceeding 0.88. The spatial overlay analysis revealed that aquaculture ponds constituted the most extensively affected land use category (6.09 km ², or 41.28 %) followed by cultivated aquatic (30.89 %) and water bodies (18.62 %). The integration of CDAT and U-net provides a comprehensive analytical framework for tidal flood impact analysis, thereby generating essential spatial data for data-driven disaster mitigation strategies and coastal zone management policies in vulnerable coastal environments.

How to cite: Setiawan, MSI. (2026). Tidal Flood Mapping Based on Land Use Classification Using CDAT and Deep Learning in Sayung, Demak. *Jambura Geoscience Review, 8*(1), 163-174. https://doi.org/10.37905/jgeosrev.v8i2.36629

1. INTRODUCTION

The Sayung District constitutes a coastal region in Demak Regency that directly borders Semarang City. This area is strategically important as the main transportation corridor through the Semarang–Demak North Coast Road (Pantura) and as a center for fisheries and aquaculture activities. However, this geographical position renders Sayung highly vulnerable to tidal flooding and coastal erosion. In recent decades, the coastal area has experienced significant environmental degradation, including the elimination of aquaculture land, inundated residential areas, and disrupted transportation infrastructure (Marfai et al., 2016). The intensity of tidal flooding escalated critically in 2025, with January inundation affecting the Pantura Road and February seawater reaching up to 40 cm in residential and aquaculture areas, demonstrating that tidal flooding has become a progressively intensifying phenomenon rather than a momentary occurrence.

Conventional mapping methods have critical limitations in tidal flood monitoring, including limited spatial coverage, high operational costs, and inaccessibility of inundated areas (Marfai &

King, 2008). Remote sensing offers more effective solutions through extensive, accurate, and periodic spatial data acquisition (Kuenzer et al., 2013). SAR imagery, particularly Sentinel-1A, demonstrates significant advantages over optical imagery by remaining unaffected by weather and cloud cover (Torres et al., 2012). The CDAT method has proven effective for detecting inundation dynamics through temporal SAR analysis, whereas the U-Net deep learning architecture has demonstrated superior performance in land use classification by preserving spatial details through its encoder–decoder structure with skip connections (Haile et al., 2023; Nair et al., 2024; Li et al., 2024). The fusion of Sentinel-1 and Sentinel-2 sensors further enhances the classification of spectrally similar coastal land use classes (Solórzano et al., 2021).

Despite these advances, three critical gaps persist in the literature. First, tidal flood mapping studies have predominantly relied on single-sensor imagery and focused solely on flood extent delineation without quantifying the impacts on specific land use categories (Tran et al., 2022). Second, land use classification in coastal areas has been conducted independently from flood detection workflows, limiting integrated spatial impact analysis. Third, deep learning hyperparameters have rarely been systematically optimized, constraining classification accuracy in spectrally complex coastal environments (Clark et al., 2023). This study addresses these gaps by integrating the CDAT method with a U-Net deep learning model trained on stacked Sentinel-1A and Sentinel-2A data, with systematic hyperparameter optimization within a unified spatial analysis framework.

This study aimed to map the spatial distribution of tidal flooding and quantify its impacts on land use in the Sayung District through integrated CDAT flood detection and U-Net-based land use classification. The scope encompasses a temporal analysis of 2025 tidal flooding events, multi-sensor image processing, hyperparameter optimization, and spatial overlay analysis to support evidence-based disaster mitigation and sustainable coastal spatial planning policies.

2. METHOD

2.1. Research Design

This study employs a quantitative design with remote sensing and machine learning approaches to achieve two primary objectives: detecting tidal flood extents using change detection and thresholding (CDAT), and classifying land use types in flood-affected areas using a U-Net. The research flowchart is presented in Figure 1.

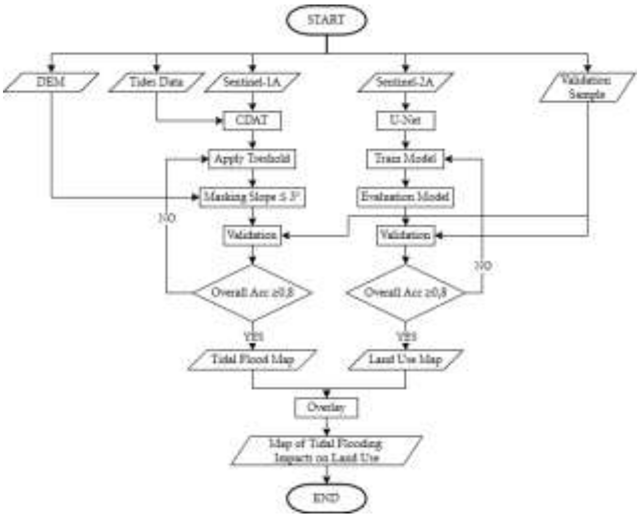

Figure 1. Research Flowchart

2.2. Study Area

This study was conducted in the Sayung District, Demak Regency, Central Java Province, Indonesia. This site was selected based on recurrent tidal flooding events that have significantly impacted the area over the past decade. The study area is approximately located at 6°51'31"–6°59'17" S latitude and 110°27'24"–110°33'47″ E longitude.

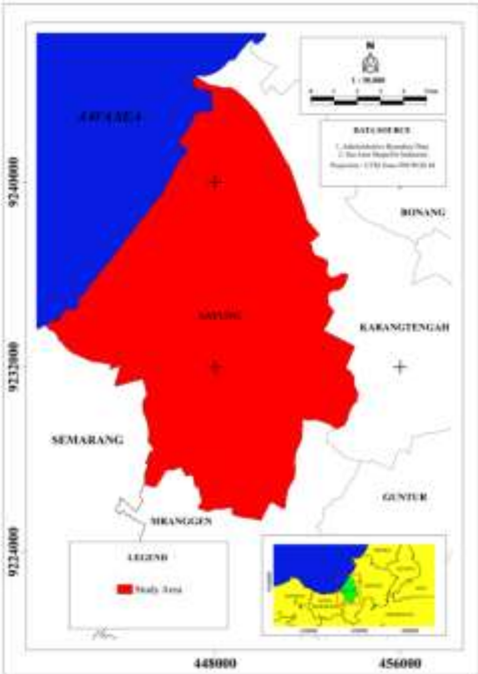

Figure 2. Map of Study Area

2.3. Data

The data used in this study are presented in Table 1.

Table 1. Research Data

Data	Source	Years
Administrative and coastline boundaries	https://tanahair.indonesia.go.id/	2020
DEMNAS	https://tanahair.indonesia.go.id/	2025
Sentinel-1A	Google Earth Engine	2025
Sentinel-2A	Google Earth Engine	2025
Tidal data	BMKG Semarang Maritime Station	2025
Validation data	Field survey	2025

2.4. Change Detection and Thresholding Method

The CDAT method was employed to map tidal flood extents using Sentinel-1A imagery acquired in two temporal phases: a dry-condition image obtained on June 18, 2025, and a flood-condition image obtained on May 11, 2025, both in the ascending orbit direction with vertical (VH) horizontal (IW) polarization, and interferometric wide (IW) acquisition mode. Pre-processing involved radiometric calibration to convert digital numbers to backscatter coefficients (σ^0) on a decibel scale, followed by speckle filtering using a Lee filter with a 5×5 window to reduce noise, and range–doppler terrain correction using DEMNAS data resampled to 10 meter resolution to ensure geometric accuracy. Normalization was subsequently applied to standardize backscatter values across both temporal images prior to change detection. Change detection computed the backscatter difference between the two temporal images using Equation (1).

$$\Delta\sigma^\circ = \sigma^\circ\text{flood} - \sigma^\circ\text{dry} \quad (1)$$

where $\Delta\sigma^\circ$ represents the backscatter change, σ°flood denotes the backscatter coefficient under flood conditions, and σ°dry indicates the backscatter coefficient under dry conditions.

Threshold determination utilized the Otsu method, which automatically computes the optimal threshold based on inter-class variance maximization from histogram analysis, as described by Yousefi (2011):

$$\sigma_B{}^2(t) = \omega_0(t) \cdot \omega_1(t) \cdot \left(\mu_0(t) - \mu_1(t)\right)^2 \quad (2)$$

where 〖σ_B〗^2 (t) represents inter-class variance for threshold t, $\omega_0(t)$ denotes background class probability, $\omega_1(t)$ indicates foreground class probability, $\mu_0(t)$ signifies mean pixel intensity of background, and $\mu_1(t)$ represents mean pixel intensity of foreground. The initial Otsu threshold was subsequently adjusted by applying a -0.5 dB offset to minimize false positive detections arising from soil moisture variations and non-inundation surface changes, following empirical calibration procedures consistent with SAR-based flood mapping practices (Haile et al., 2023). Areas with slopes ≤8% derived from the DEMNAS terrain analysis were additionally classified as flood-prone zones to refine inundation mapping (Watson et al., 2024; Tariq et al., 2022;).

2.5. Land Use Classification Using U-Net

The U-Net architecture was implemented for multi-class land use classification using combined Sentinel-1A and Sentinel-2A data. U-Net, originally proposed by Ronneberger et al. (2015), employs a symmetrical encoder-decoder structure with skip connections that preserve spatial details during feature extraction, making it particularly suitable for semantic segmentation tasks in remote sensing applications. The combination of Sentinel-1A (VV and VH) with Sentinel-2A (red, green, blue, near infrared, and shortwave infrared-1) enables the model to learn effectively and achieve high performance in land use mapping (Solórzano et al., 2021). The dataset was partitioned into three subsets: train (70%) for model training, validation (20%) for validation during training, and test (10%) for final evaluation. Data augmentation included flipping and rotation. Normalization scaled Sentinel-2A and Sentinel-1A to the range of 0–1. The addition of NDVI, NDWI, and NDBI indices has been proven to assist the model in distinguishing vegetation classes from water bodies and built-up land, thereby improving segmentation quality (Nair et al., 2024):

$$\mathrm{NDVI} = \frac{(\mathrm{NIR} - \mathrm{Red})}{(\mathrm{NIR} + \mathrm{Red})} \tag{3}$$

$$\mathrm{NDWI} = \frac{(\mathrm{Green} - \mathrm{NIR})}{(\mathrm{Green} + \mathrm{NIR})} \tag{4}$$

$$\mathrm{NDBI} = \frac{(\mathrm{SWIR} - \mathrm{NIR})}{(\mathrm{SWIR} + \mathrm{NIR})} \tag{5}$$

The model architecture utilized input dimensions of (128, 128, 10) with an encoder–decoder structure: four encoder blocks (max pooling), bottleneck layer (dropout at 0.5), and four decoder blocks (skip connections). Each block contained two Conv2D (3×3), batch normalization, ReLU activation, and L2 regularization (1e-4), with a softmax output for a 12-class prediction. A dropout rate of 0.5 and L2 regularization (1e-4) were applied to prevent overfitting in the limited training dataset, consistent with recommendations for deep learning applied to remote sensing data (Goodfellow et al., 2016). A patch size of 128×128 pixels was selected to balance spatial context preservation and computational efficiency. Training employed the Adam optimizer (learning rate 0.001), a custom loss that ignored the undefined class, a batch size of 8, a maximum of 150 epochs, ModelCheckpoint, and EarlyStopping (with a patience of 15). The prediction utilized a tile-based approach with 128×128 pixels.

2.6. Evaluation Model

Model performance was assessed using three quantitative metrics. Pixel accuracy computes the overall classification accuracy as the ratio of correctly classified pixels to the total sample pixels used in model evaluation (Goodfellow et al., 2016):

$$\text{Pixel Accuracy} = \frac{\sum_{i=1}^{k} n_{ii}}{\sum_{i=1}^{k}\sum_{j=1}^{k} n_{ij}} \times 100\% \tag{6}$$

where n_{ii} denotes the number of pixels correctly classified for class i (prediction matches the ground truth label), n_{ij} represents the number of predicted pixels for class i that actually originate from class j, and k indicates the total number of classes used in the classification process.

Intersection over Union (IoU) measures the ratio of the intersection area to the union area between the prediction and ground truth (Badrinarayanan et al., 2015):

$$\mathrm{IoU} = \frac{|A \cap B|}{|A \cup B|} \tag{7}$$

where A represents the predicted pixel set, B denotes the ground truth label pixel set, $|A \cap B|$ indicates the intersection area, and $|A \cup B|$ signifies the union area.

The Dice coefficient quantifies the similarity between a prediction and the ground truth, with better performance for imbalanced classes (Sudre et al., 2017):

$$\mathrm{Dice} = \frac{2TP}{2TP + FP + FN} \tag{8}$$

where TP (true positive) represents correctly classified pixels as the target class (positive prediction and positive label), FP (false positive) denotes incorrectly classified pixels as the target class when they are not part of that class (positive prediction, negative label), and FN (false negative) indicates pixels not classified as the target class when they actually belong to it (negative prediction, positive label).

2.7. Sampling Technique and Field Validation

Field validation was conducted on July 12, 2025, utilizing 70 sampling points selected through modified stratified random sampling. Modifications were necessitated by accessibility constraints, including infrastructure development, road closures, and permanently inundated zones. The sampling point distribution considered land use variability, flood intensity, and spatial representation across the coastal area. Ground truth data collection comprised direct field observations to identify land use types and tidal flood traces, and structured interviews with local residents regarding flood frequency, inundation duration, and impacts on agricultural and residential activities.

2.8. Spatial Analysis and Validation

Spatial overlay analysis employed the intersect technique to combine tidal flood extent maps with land use classification maps, thereby obtaining detailed information on the area and distribution of each affected land use class. The analysis results were visualized as thematic maps and statistical tables, showing the flood impact distribution across various land-use categories. Validation accuracy was assessed using a confusion matrix that compared field observation results with model predictions to evaluate classification reliability and identify error sources. Classification error analysis was conducted to understand misclassification patterns and provide recommendations for future model improvements.

3. RESULTS AND DISCUSSION

3.1. Results

This study encompasses three main components which include tidal flood inundation mapping using CDAT, land use classification employing a deep learning model based on U-Net architecture, and impact analysis of tidal flooding on various land use classes in Sayung District in 2025.

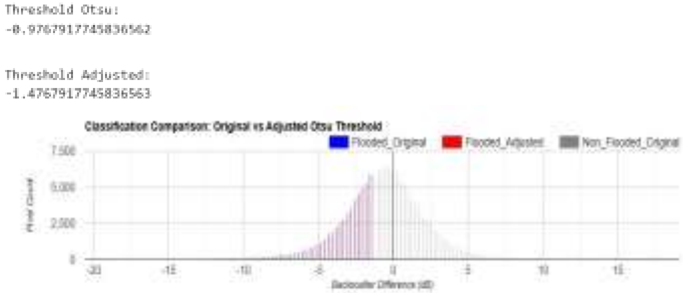

Figure 3. Histogram distribution with Otsu threshold for tidal flood detection.

The histogram distribution of VH counts, as shown in Figure 3, displays a near-normal distribution pattern centered around zero. The Otsu threshold (τ = − 0.977) was automatically calculated to distinguish between flooded and non-flooded areas, whereas the adjusted threshold (τ = − 1.476) was implemented to reduce classification errors and improve flood extent delineation.

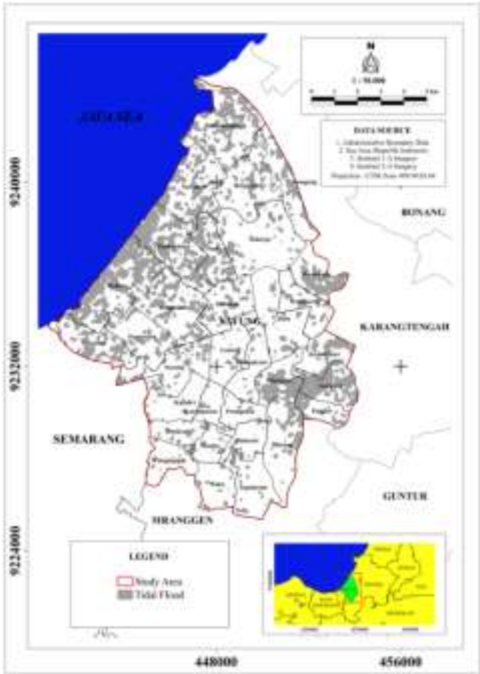

Figure 4. Map of Flood Inundation Areas.

The tidal flood inundation mapping using the CDAT method, as illustrated in Figure 4, reveals that in 2025, the inundation area reached 32.21 km² (31.62%) of the total area of the Sayung District. The most extensive inundation was identified in the Bedono Subdistrict (4 km², or 55 %), followed by Timbulsloko (3 km², or 51 %), which are located in the coastal zone and predominantly characterized by aquaculture ponds. The threshold analysis using the Otsu algorithm produced an initial threshold of -0.98 dB, which was then adjusted to–1.47 dB to reduce false-positive detections and improve classification accuracy.

Table 2. Validation Assessment of the Inundation Model

Confusion Matrix	Results
Overall Accuracy	0.823
Kappa Accuracy	0.634

The validation assessment of the inundation model utilizing the confusion matrix method (Table 2) yielded an overall accuracy of 0.823 and a kappa coefficient of 0.634, which was categorized as substantial agreement (Landis & Koch, 1977).

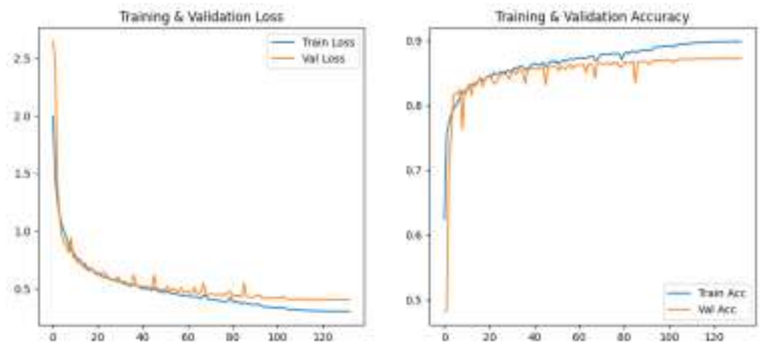

Figure 5. Training and Validation Performance of the U-Net Model.

The performance results of the U-Net model presented in Figure 5 demonstrate that the training process was conducted over 133 epochs, with the training loss reaching its optimal point at epoch 118. The training curves exhibit good convergence without any indication of overfitting. The training accuracy achieved was 0.89, whereas the validation accuracy remained stable within the range of 0.87–0.88, indicating consistent and balanced model performance between the training and validation datasets.

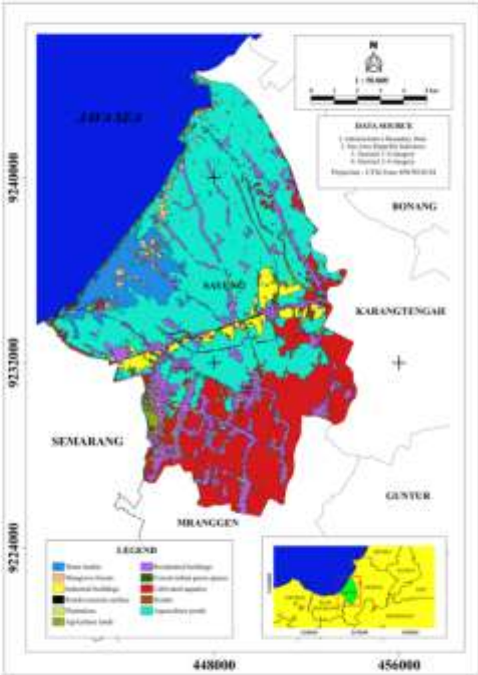

Figure 6. Map of Land Use Classifications

The land use classification results using the U-Net model, presented in Figure 6, indicate that the fish pond class dominates land use in the Sayung District, covering an area of 66.78 km² (49.32%).

Table 3. Performance Metrics of U-Net Model across Land Use Classes

Land Use	Pixel Accuracy	IoU	Dice Coefficient
Water bodies	0.603	0.512	0.677
Mangrove forests	0.583	0.467	0.636
Forests	0.113	0.103	0.186
Industrial buildings	0.783	0.644	0.783
Roads/concrete surface	0.273	0.205	0.34
Plantations	0.451	0.328	0.494
Agriculture lands	0.665	0.505	0.671
Residential buildings	0.837	0.648	0.787
Cultivated aquatics	0.969	0.883	0.938
Scrubs	0.31	0.246	0.395
Aquaculture ponds	0.964	0.892	0.943

Model performance was evaluated using three quantitative metrics: Pixel Accuracy, IoU, and Dice Coefficient, computed programmatically on the test dataset split (Table 3). The aquaculture pond class achieved the highest IoU of 0.892 and Dice Coefficient of 0.943, followed by cultivated aquatics with IoU of 0.883 and Dice Coefficient of 0.938, reflecting the model's strong capability in distinguishing dominant coastal land use classes. In contrast, the forest class recorded the lowest performance across all metrics (IoU = 0.103), likely due to limited training samples and spectral similarity with surrounding vegetation.

Table 4. Cross-Validation Performance of U-Net Model

Evaluation Models	Fold 1	Fold 2	Fold 3	Fold 4	Fold 5	Mean	Total STDEV
Pixel Accuracy	0.897	0.899	0.892	0.903	0.899	0.899	0.0037
IoU	0.603	0.617	0.610	0.614	0.594	0.608	0.0081
Dice Coefficient	0.713	0.722	0.717	0.719	0.705	0.715	0.0059

To ensure model robustness and generalizability, a 5-fold cross-validation was performed on the training dataset, in which each fold used 80% of the samples for model fitting and 20% for internal validation (Table 4). The results demonstrated consistency across all folds, with a mean pixel accuracy of 0.899 (±0.0037), mean IoU of 0.608 (±0.0081), and mean Dice coefficient of 0.715 (±0.0059), confirming stable model performance with minimal variation.

Table 5. U-Net Model Accuracy

Confusion Matrix	Results
Overall Accuracy	0.81
Kappa Accuracy	0.78

The validation assessment of the U-Net model utilizing the confusion matrix method (Table 5) yielded an overall accuracy of 0.81 and a kappa coefficient of 0.78, which was categorized as substantial agreement (Landis & Koch, 1977).

The three evaluation settings employed in this study reflect progressively independent assessments: the per-class metrics in Table 3 evaluate performance on the computational test split, cross-validation in Table 4 assesses internal training consistency, and the field-based confusion matrix in Table 5 evaluates real-world generalizability. The discrepancy between the cross-validation pixel accuracy (~0.899) and field-validated overall accuracy (~0.81) is expected, as the former operates within the training data distribution, whereas the latter reflects generalization to actual ground conditions.

Overlay analysis between tidal flooding inundation and land use indicates that the three most affected types of land use are aquaculture ponds (41.28%), cultivated aquatics (30.89%), and water bodies (18.62%), as illustrated in Figure 7.

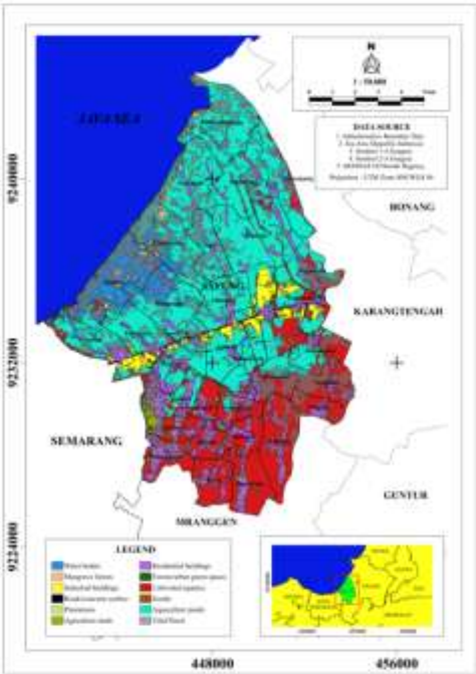

Figure 7. Map of Land Use Impacted Areas

3.2. Discussion

This study demonstrates that the integration of change detection and thresholding (CDAT) with U-Net-based land use classification provides an effective framework for detecting and assessing tidal flood impacts in the Sayung District. The CDAT method identified 32.21 km² of inundated area, equivalent to 31.62% of the district, indicating that tidal flooding remains a substantial coastal hazard in this region. The spatial pattern of inundation was concentrated in low-lying coastal villages, particularly Bedono, Timbulsloko, Tambakbulusan, Surodadi, Sampang, and Sidogemah, confirming that elevation and proximity to the coastline strongly influence tidal flood exposure.

Adjusting the Otsu-derived threshold from −0.98 to −1.47 dB was essential for improving the delineation of inundation. The initial threshold tended to overestimate the flooded areas by including pixels affected by soil moisture variations, agricultural activities, or other non-flood surface changes. By applying the adjusted threshold, the CDAT method selectively captured pixels with substantial VH backscatter reductions, which is characteristic of the water surface in SAR imagery. This optimization resulted in an overall accuracy of 82.3% and a kappa coefficient of 0.634, indicating substantial agreement, as described by Landis and Koch (1977). Therefore, the adjusted threshold improved the reliability of tidal flood detection while reducing the number of false-positive classifications.

The land use classification using the U-Net model also exhibited strong performance, with a training accuracy of 0.89 and a validation accuracy ranging from 0.87 to 0.88. These values indicate adequate model learning without strong evidence of overfitting, consistent with the acceptable performance range for deep learning models described by Goodfellow et al. (2016). The combination of Sentinel-1A, Sentinel-2A, and spectral indices, such as NDVI, NDWI, and NDBI, improved the model's ability to distinguish land use classes, supporting previous findings on the effectiveness of multisource remote sensing data for land cover classification (Nair et al., 2024; Solórzano et al., 2021; Vizzari et al., 2022; Amalia & Benardi, 2026).

The U-Net model achieved an overall accuracy of 0.81 and a Kappa coefficient of 0.78, outperforming conventional machine learning approaches such as Random Forest and SVM. This improvement is mainly attributed to the capability of U-Net to capture spatial context and hierarchical features, which is particularly important for distinguishing spectrally similar classes such as aquaculture ponds and cultivated aquatics. This finding is consistent with Boston et al. (2022), who reported that deep learning-based segmentation provides advantages over pixel-based classification methods in complex landscapes.

The overlay between inundation and land use revealed that aquaculture ponds were the most affected class, accounting for 41.28% of the inundated area, followed by cultivated aquatics (30.89 %) and water bodies (18.62 %). This pattern indicates that productive coastal land uses are highly vulnerable to tidal flooding because they are commonly located in low-elevation zones with direct exposure to tidal intrusions. Although the impacts on residential buildings are smaller in area, they remain significant because they are associated with risks to settlement safety, infrastructure stability, and community livelihood. These findings are consistent with those of Diana et al. (2024), who emphasized that flooding in agricultural and infrastructure areas can reduce productivity and disturb ecosystem stability.

The results also support previous findings that Sayung is one of the most vulnerable coastal areas in Demak, owing to its flat topography, land subsidence, and exposure to seawater intrusion (Khairullah et al., 2024). However, this study provides additional methodological value by combining automated SAR-based flood detection with deep learning-based land use classification. This integration enables more detailed quantification of tidal flood impacts across land use classes and provides spatially explicit information for coastal disaster mitigation.

The findings have important implications for coastal management. The high exposure of aquaculture ponds and cultivated aquatics indicates the need for adaptive land use planning, improved drainage systems, protective embankments, and climate-resilient aquaculture practices. The inundation of mangrove areas further highlights the urgency of mangrove restoration, as the degradation of this ecosystem can weaken natural coastal protection and increase future flood vulnerability. Therefore, the integrated CDAT–U-Net approach can support early warning systems, spatial planning, and long-term monitoring of coastal vulnerability.

Despite its advantages, this study has several limitations. The temporal mismatch between the Sentinel-1A acquisition and peak tidal events may have caused an underestimation of the inundation extent. The 10–20 m spatial resolution also limits the detection of small objects, such as narrow roads and minor land cover patches. Future studies should integrate higher-resolution imagery, improve temporal data acquisition strategies, apply advanced architectures such as U-Net++ or ELU-Net, and address class imbalance using methods such as focal loss or enriched training samples. These improvements would further enhance the accuracy and operational applicability of tidal flood monitoring in coastal regions.

4. CONCLUSIONS

This study successfully assessed and mapped the spatial distribution of tidal flooding and quantified its impacts on land use in the Sayung District through the integrated application of remote sensing and deep learning methods. The CDAT method using Sentinel-1A imagery detected 32.21 km² of inundated area, representing 31.62% of the study area, with an overall accuracy of 82.3% and a Kappa coefficient of 0.634. Meanwhile, the U-Net model, developed using stacked Sentinel-1A and Sentinel-2A data, classified eleven land use categories with an overall accuracy of 0.81 and a kappa coefficient of 0.78. Spatial overlay analysis revealed that aquaculture ponds were the most extensively affected land use category, followed by cultivated aquatic areas and residential buildings, thereby addressing the research gap related to integrated flood detection and land use impact assessment.

The main novelty of this study lies in the synergistic integration of CDAT-based tidal flood detection and U-Net-based multiclass land use classification. This dual-method framework enables the simultaneous delineation of inundation extent and identification of affected land use types, offering a more comprehensive analytical approach than conventional single-method assessments. The results provide essential spatial evidence to support disaster mitigation, coastal zone management, and sustainable spatial planning in the Sayung District and other vulnerable coastal regions.

Nevertheless, this study has several limitations. The analysis was based on two temporal image acquisitions, which may not fully represent seasonal variability and long-term tidal flood dynamics. In addition, the lower classification performance for certain classes, particularly forests and roads, indicates the need for improved ground truth quality and more representative training samples. Future studies should incorporate multi-temporal imagery, tide gauge records, and land subsidence data, as well as test the transferability of the proposed framework in other coastal environments.

5. REFERENCES

Amalia, S., & Benardi, A. (2026). Spatiotemporal Analysis Of Flood Inundation Using MNDWI At Rawa Pening 2019-2025. *Jambura Geoscience Review, 8*(1), 94-107. doi:https://doi.org/10.37905/jgeosrev.v8i1.35670

Badrinarayanan, V., Kendall, A., & Cipolla, R. (2017). SegNet: A deep convolutional encoder-decoder architecture for image segmentation. *IEEE Transactions on Pattern Analysis and Machine Intelligence, 39*(12), 2481–2495. https://doi.org/10.1109/TPAMI.2016.2644615

Boston, T., Van Dijk, A., Larraondo, P. R., & Thackway, R. (2022). Comparing CNNs and random forests for Landsat image segmentation trained on a large proxy land cover dataset. *Remote Sensing, 14*(14), 3396. https://doi.org/10.3390/rs14143396

Clark, A., Phinn, S., & Scarth, P. (2023). Optimised U-Net for land use–land cover classification using aerial photography. *PFG – Journal of Photogrammetry, Remote Sensing and Geoinformation Science, 91*(2), 125–147. https://doi.org/10.1007/s41064-023-00233-3

Clement, M. A., Kilsby, C. G., & Moore, P. (2018). Multi-temporal synthetic aperture radar flood mapping using change detection. *Journal of Flood Risk Management, 11*(2), 152–168. https://doi.org/10.1111/jfr3.12303

Diana, Z. A., Saputri, D. E., Arifin, B., & Huda, A. N. (2024). Dampak banjir rob terhadap perekonomian warga Desa Loireng Kecamatan Sayung Kabupaten Demak. *Jurnal Alwatzikhoebillah: Kajian Islam, Pendidikan, Ekonomi, Humaniora, 10*(1), 194–200. https://doi.org/10.37567/alwatzikhoebillah.v10i1.2552

Goodfellow, I., Bengio, Y., & Courville, A. (2016). *Deep learning*. MIT Press.

Haile, A. T., Bekele, T. W., & Rientjes, T. (2023). Interannual comparison of historical floods through flood detection using multi-temporal Sentinel-1 SAR images, Awash River Basin, Ethiopia. *International Journal of Applied Earth Observation and Geoinformation, 124*, 103505. https://doi.org/10.1016/j.jag.2023.103505

Kasanah, N., Bashit, N., & Hadi, F. (2020). Analisis lahan sawah tergenang banjir menggunakan metode change detection dan PPPM (*Phenology and Pixel Based Paddy Rice Mapping*): Studi kasus Kabupaten Demak. *Jurnal Geodesi Undip, 10*(1), 259–268. https://doi.org/10.14710/jgundip.2021.29713

Khairullah, K. K., Rifai, A., & Indrayanti, E. (2024). Studi luasan genangan banjir rob akibat kenaikan muka air laut dan penurunan muka tanah di Kecamatan Sayung, Demak. *Indonesian Journal of Oceanography, 6*(4), 316–323. https://doi.org/10.14710/ijoce.v6i4.24645

Kuenzer, C., Guo, H., Huth, J., Leinenkugel, P., Li, X., & Dech, S. (2013). Flood mapping and flood dynamics of the Mekong Delta: ENVISAT-ASAR-WSM based time series analyses. *Remote Sensing, 5*(2), 687–715. https://doi.org/10.3390/rs5020687

Landis, J., & Koch, G. (1977). An application of hierarchical kappa-type statistics in the assessment of majority agreement among multiple observers. *Biometrics, 33*, 363–374. https://doi.org/10.2307/2529786

Li, Z., Chen, B., Wu, S., Su, M., Chen, J. M., & Xu, B. (2024). Deep learning for urban land use category classification: A review and experimental assessment. *Remote Sensing of Environment, 311*, 114290. https://doi.org/10.1016/j.rse.2024.114290

Marfai, M. A., & King, L. (2008). Tidal inundation mapping under enhanced land subsidence in Semarang, Central Java, Indonesia. *Natural Hazards, 44*(1), 93–109. https://doi.org/10.1007/s11069-007-9144-z

Marfai, M. A., Tyas, D. W., Nugraha, I., Fitriatul'Ulya, A., & Riasasi, W. (2016). The morphodynamics of Wulan Delta and its impacts on the coastal community in Wedung Subdistrict, Demak Regency, Indonesia. *Journal of Environmental Protection, 7*(1), 60–71. https://doi.org/10.4236/jep.2016.71006

Nair, S., Sharifzadeh, S., & Palade, V. (2024). Farmland segmentation in Landsat 8 satellite images using deep learning and conditional generative adversarial networks. *Remote Sensing, 16*(5), 283. https://doi.org/10.3390/rs16050823

Pushpalatha, V., Mallikarjuna, P., Mahendra, H., Subramoniam, S. R., & Mallikarjunaswamy, S. (2025). Land use and land cover classification for change detection studies using convolutional neural network. *Applied Computing and Geosciences, 25*, 100227. https://doi.org/10.1016/j.acags.2025.100227

Ronneberger, O., Fischer, P., & Brox, T. (2015). U-Net: Convolutional networks for biomedical image segmentation. In *Medical Image Computing and Computer-Assisted Intervention – MICCAI 2015* (Vol. 9351, pp. 234–241). Springer. https://doi.org/10.1007/978-3-319-24574-4_28

Schumann, G. J.-P., Brakenridge, G. R., Kettner, A. J., Kashif, R., & Niebuhr, E. (2018). Assisting flood disaster response with Earth observation data and products: A critical assessment. *Remote Sensing, 10*(8), 1230. https://doi.org/10.3390/rs10081230

Solórzano, J. V., Mas, J. F., Gao, Y., & Gallardo-Cruz, J. A. (2021). Land use land cover classification with U-Net: Advantages of combining Sentinel-1 and Sentinel-2 imagery. *Remote Sensing, 13*(18), 3600. https://doi.org/10.3390/rs13183600

Sudre, C. H., Li, W., Vercauteren, T., Ourselin, S., & Cardoso, M. J. (2017). Generalised Dice overlap as a deep learning loss function for highly unbalanced segmentations. In *Deep Learning in Medical Image Analysis and Multimodal Learning for Clinical Decision Support* (Vol. 10553, pp. 240–248). Springer. https://doi.org/10.1007/978-3-319-67558-9_28

Tariq, A., Yan, J., Ghaffar, B., Qin, S., Mousa, B. G., Sharifi, A. S., ... Aslam, M. (2022). Flash flood susceptibility assessment and zonation by integrating analytic hierarchy process and frequency ratio model with diverse spatial data. *Water, 14*(19), 3069. https://doi.org/10.3390/w14193069

Torres, R., Snoeij, P., Geudtner, D., Bibby, D., Davidson, M., Attema, E., ... Rostan, F. (2012). GMES Sentinel-1 mission. *Remote Sensing of Environment, 120*, 9–24. https://doi.org/10.1016/j.rse.2011.05.028

Tran, K. H., Menenti, M., & Jia, L. (2022). Surface water mapping and flood monitoring in the Mekong Delta using Sentinel-1 SAR time series and Otsu threshold. *Remote Sensing, 14*(22), 5721. https://doi.org/10.3390/rs14225721

Vizzari, M. (2022). PlanetScope, Sentinel-2, and Sentinel-1 data integration for object-based land cover classification in Google Earth Engine. *Remote Sensing, 14*(11), 2628. https://doi.org/10.3390/rs14112628

Watson, C. S., Gyawali, J., Creed, M., & Elliott, J. R. (2024). City-scale high-resolution flood models and the role of topographic data: A case study of Kathmandu, Nepal. *Geocarto International, 39*(1), 2387073. https://doi.org/10.1080/10106049.2024.2387073

Yousefi, J. (2011). *Image binarization using Otsu thresholding algorithm* [Technical report]. University of Guelph. https://doi.org/10.13140/RG.2.1.4758.9284